Systematic effects in two-dimensional trapped matter-wave interferometers

Adam D. West*

UCLA, Department of Physics and Astronomy, 475 Portola Plaza, Los Angeles, California 90095, USA

(Received 8 May 2019; published 9 December 2019)

Trapped matter-wave interferometers (TMIs) present a platform for precision sensing within a compact apparatus, extending coherence time by repeated traversal of a confining potential. However, imperfections in this potential can introduce unwanted systematic effects, particularly when combined with errors in the associated beam-splitter operations. This can affect both the interferometer phase and visibility, and can make the performance more sensitive to other experimental imperfections. I examine the character and degree of these systematic effects, in particular within the context of two-dimensional TMIs applicable for rotation sensing. I show that current experimental control can enable these interferometers to operate in a regime robust against experimental imperfections.

DOI: 10.1103/PhysRevA.100.063622

I. INTRODUCTION

Matter-wave interferometry with ultracold atoms has proven to be a powerful tool for precision sensing of numerous physical quantities [1] such as gravitational acceleration [2–4], the gravitational constant [5], rotations [6–9], and various atomic properties [10–12]. It has also been used in searches for new physics [13,14]. Many such experiments embody some version of the Ramsey method [15], where sensing of the quantity of interest occurs during a "free-evolution" time. In most matter-wave interferometers, this takes the form of a period of "free flight," where the wave packets are isolated from external fields which could contribute to the measured interferometer phase. This isolation, together with the precise control of atom-light interactions, affords atom interferometers their exquisite accuracy. However, imperfections such as vibrations, velocity spread, and residual external fields can still cause systematic effects [16,17].

By contrast, the free evolution in trapped matter-wave interferometers (TMIs) occurs within a confining potential, typically with either a toroidal [18–21] or harmonic [22–25] geometry. In this paper, I will focus on the latter. The TMI paradigm offers the benefit of an extended interaction time in a compact apparatus as well as the ability to use charged species—extremely challenging in conventional free flight interferometers. TMIs also provide resilience to systematics: for harmonic potentials, the accumulated phase has zero contribution from the confining potential and is insensitive to the initial velocity of the wave packets. However, this demands that the confining potential is well controlled [26]. The common-path geometry also makes TMIs generally less sensitive to external forces, e.g., from vibrations or external fields. This insensitivity makes them ideally suited to rotation sensing through Sagnac interferometry [27,28], an area of significant recent interest [21,28–30]. Free-flight matter-wave interferometers can provide precise rotation measurements [7,9,31,32], but typically require large apparatuses with relatively low measurement bandwidth (recent experiments in free-flight interferometers have made significant improvements in this regard [33]). In this paper, I investigate the technical requirements for effective operation of TMIs with harmonic confinement, in particular examining the control of the matter-wave packets and the associated trapping potential.

II. TRAPPED MATTER-WAVE INTERFEROMETRY

A. Interferometer sequence

In this section, I describe the general interferometer sequence under consideration, based largely on current work to develop an ion-based TMI [24]. For simplicity, the treatment is restricted to two spatial dimensions. In Sec. II A 2, I describe the method for computing wave-packet trajectories and the associated phases. The corresponding interferometer visibility can be computed by direct relation to a coherent-state description of the wave packets.

1. Coherent-state formalism

I shall describe the evolution of the interferometer's wave packets in the basis of coherent states. First, I consider the case of a one-dimensional (1D) interferometer. The result is easily extended to higher dimensionality. A harmonically confined particle is assumed to be initially in a coherent motional state (extension to thermal states is considered later) and a pure spin state,

$$|\psi_0\rangle = |\alpha\rangle \otimes |\uparrow\rangle \equiv |\alpha, \uparrow\rangle. \tag{1}$$

I work in an interaction picture such that phases associated with the time evolution of the internal states are not considered. The coherent state $|\alpha\rangle$ is defined by a complex number α that describes the expectation values of position and momentum,

$$\langle\alpha|x|\alpha\rangle = \sqrt{\frac{2\hbar}{m\omega}}\ \mathrm{Re}(\alpha), \tag{2}$$

$$\langle\alpha|p|\alpha\rangle = \sqrt{2m\omega\hbar}\ \mathrm{Im}(\alpha), \tag{3}$$

*adam@physics.ucla.edu

where m is the mass of the particle and ω is the trap frequency. The state $|\alpha\rangle$ can be expressed in terms of Fock states ("number" states) $|n\rangle$, as

$$|\alpha\rangle = e^{-|\alpha|^2/2} \sum_n \frac{\alpha^n}{\sqrt{n!}} |n\rangle. \tag{4}$$

The internal state is prepared in a superposition by application of a $\pi/2$ pulse,

$$\mathcal{R}_{\pi/2} \equiv \frac{1}{\sqrt{2}}[(|\uparrow\rangle + |\downarrow\rangle)\langle\uparrow| + (|\uparrow\rangle - |\downarrow\rangle)\langle\downarrow|]. \tag{5}$$

A series of state-dependent kicks (SDKs) is performed at time $t = 0$, splitting the wave packet into two and entangling the spin and motion, generating two distinct momentum states. This can be represented by the following operator:

$$\mathcal{D}_{\mathrm{SDK}}[in_{\mathrm{k}}\eta] \equiv \mathcal{D}[in_{\mathrm{k}}\eta]|\uparrow\rangle\langle\uparrow| + \mathcal{D}[-in_{\mathrm{k}}\eta]|\downarrow\rangle\langle\downarrow|, \tag{6}$$

where n_{k} is the number of kicks applied and η is the associated Lamb-Dicke parameter, given by

$$\eta = k\sqrt{\frac{\hbar}{2m\omega}}, \tag{7}$$

where k is the effective wave vector for the transition. The displacement operator $\mathcal{D}$ is defined as

$$\mathcal{D}[\beta]|\alpha\rangle \equiv e^{\beta\hat{a}^\dagger - \beta^*\hat{a}}|\alpha\rangle = e^{(\beta\alpha^* - \beta^*\alpha)/2}|\alpha + \beta\rangle. \tag{8}$$

Following the SDKs, the wave packets evolve freely in the trap for some time t_{free}. In the ideal case, the evolution time is a multiple of the trap period, $\tau = 2\pi/\omega$, and the wave packets return to their initial positions in phase space. Imperfections which lead to a residual separation of the wave packets cause a reduction in visibility. I represent such an effect as an additional spin-dependent phase-space displacement of the wave packets:

$$\mathcal{D}_{\mathrm{imp}} \equiv \mathcal{D}[\delta_\uparrow]|\uparrow\rangle\langle\uparrow| + \mathcal{D}[\delta_\downarrow]|\downarrow\rangle\langle\downarrow|, \tag{9}$$

where, in general, $\delta_\downarrow \neq \delta_\uparrow$. After the free-oscillation period, another series of SDKs opposite to the first and a second $\pi/2$ pulse are performed. The final state of the system is thus given by

$$|\psi_f\rangle = \mathcal{R}_{\pi/2}\mathcal{D}_{\mathrm{SDK}}[-in_{\mathrm{k}}\eta]\mathcal{D}_{\mathrm{imp}} \times \mathcal{D}_{\mathrm{SDK}}[in_{\mathrm{k}}\eta]\mathcal{R}_{\pi/2}|\psi_0\rangle. \tag{10}$$

Given a calculation of the final state of the wave packet, one can calculate the probability of being in a particular spin state (the signal of such an interferometer) as

$$P_\uparrow(\alpha) = |\langle\uparrow|\psi_f\rangle|^2. \tag{11}$$

It is then straightforward to extract the interferometer phase and visibility.

The same procedure can be applied to the case of a 2D interferometer, in which case the initial state is written as

$$|\psi_0\rangle = |\alpha_x, \alpha_y, \uparrow\rangle, \tag{12}$$

where α_x and α_y are the coherent states for the two orthogonal spatial axes. After preparing a superposition of internal states, a real-space displacement $\mathcal{D}^y[\tilde{d}]$ is applied such that the subsequent splitting of the wave packets occurs at a position $\tilde{d}\sqrt{\frac{2\hbar}{m\omega}}\hat{y} = d\hat{y}$. This displacement is orthogonal to the previously described momentum kicks, which are assumed to be along $\pm\hat{x}$. Following recombination of the wave packets, the initial real-space displacement is reversed ($\mathcal{D}^y[-\tilde{d}]$). The upper-left plot of Fig. 1 illustrates these displacements and the resulting orbital motion of the wave packets. The final state of the system can thus be calculated as

$$|\psi_f\rangle = \mathcal{R}_{\pi/2}\mathcal{D}^y[-d]\mathcal{D}^x_{\mathrm{SDK}}[-in_{\mathrm{k}}\eta]\mathcal{D}_{\mathrm{imp}} \times \mathcal{D}^x_{\mathrm{SDK}}[in_{\mathrm{k}}\eta]\mathcal{D}^y[d]\mathcal{R}_{\pi/2}|\psi_0\rangle. \tag{13}$$

Note that the imperfections $\delta_\uparrow$ and $\delta_\downarrow$ will, in general, be in both spatial axes. Again, an expression for the internal state distribution can be extracted that allows for calculation of the associated phase and visibility.

The procedure outlined above assumes a particle that is initially in a pure coherent state. Extension to a (mixed) thermal state is provided by describing the initial state by the Glauber-Sudarshan P representation. The density matrix of the initial state of the system is given by

$$\rho = \int P(\alpha_x)P(\alpha_y)|\alpha_x, \alpha_y, \uparrow\rangle\langle\alpha_x, \alpha_y, \uparrow|d^2\alpha_x d^2\alpha_y, \tag{14}$$

$$P(\alpha) = \frac{1}{\pi\bar{n}}e^{-|\alpha|^2/\bar{n}}, \tag{15}$$

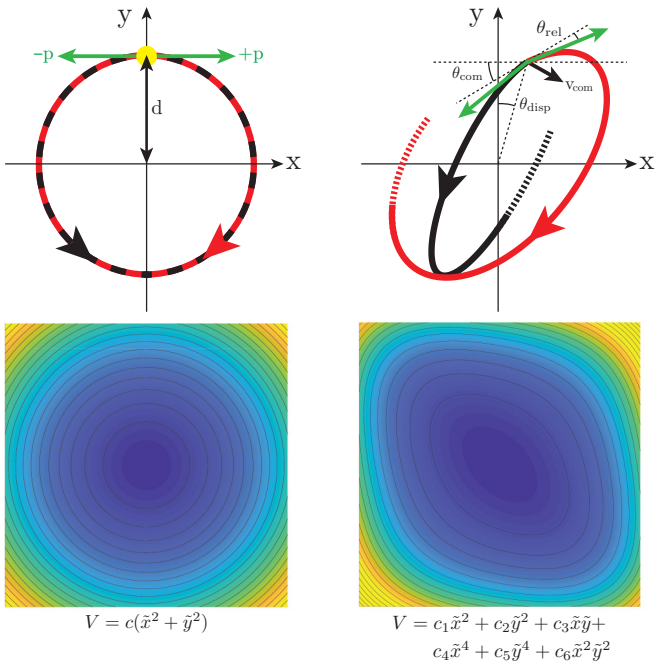

FIG. 1. Schematic of 2D interferometer sequence. The left column shows the case with no imperfections present. Top: A wave packet initially at rest a distance d from the center is split in the orthogonal direction by imparting momenta $\pm p$. The wave packets recombine at the position that they were split (yellow circle). Bottom: The ideal case assumes a purely harmonic potential. The right column shows the various imperfections that may enter the system. Top: Misalignment of the initial displacement or momenta and an initial velocity common to both wave packets. Bottom: Anharmonic imperfections to the trapping potential.

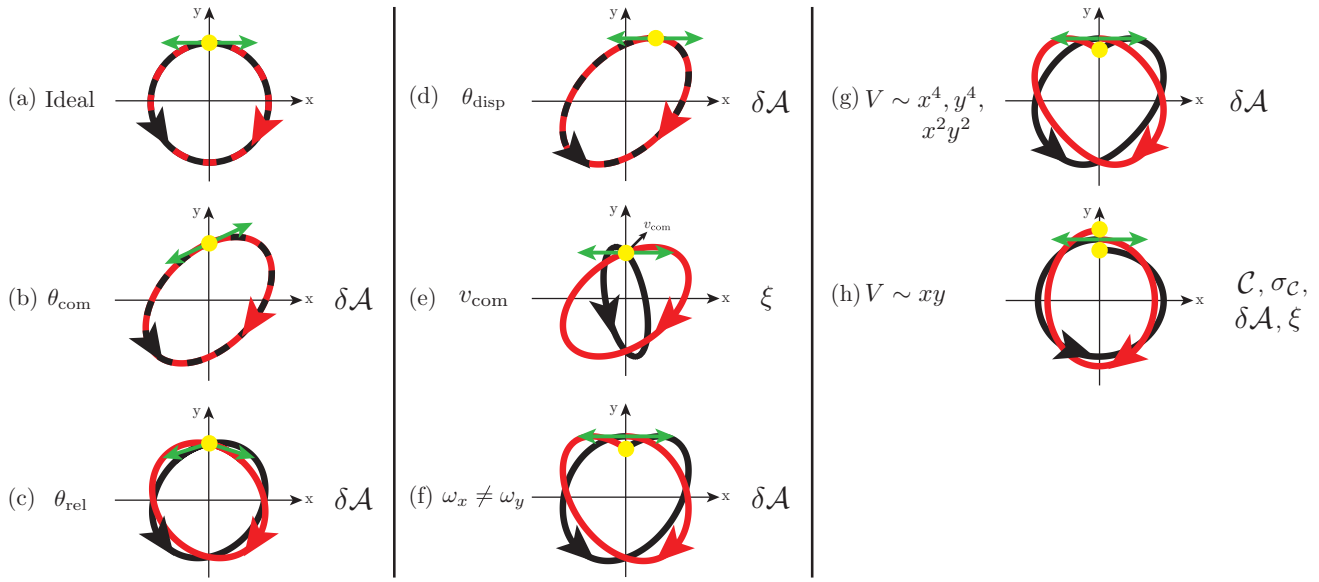

FIG. 2. Summary of the various systematic effects considered. The trajectories in real space are shown to aid intuition. Green arrows represent the directions of the imparted momenta. Yellow circles indicate points of recombination. All effects are exaggerated for clarity. The affected interferometer properties (see Sec. II B for description) are listed. (a) Ideal case; no imperfections. (b) Common misalignment of imparted momenta. (c) Relative misalignment of imparted momenta. (d) Misalignment of initial displacement. (e) Common velocity of both wave packets. (f) Mismatch in trap frequencies. (g) Anharmonicity. (h) Coupling of principal axes.

where $\bar{n}$ is the mean occupation number. The internal state distribution after the interferometry sequence can thus be extracted as

$$P_{\uparrow}^{\rm therm} = {\rm Tr}\langle\uparrow|\rho|\uparrow\rangle. \tag{16}$$

2. *Semiclassical treatment*

While the foregoing description provides a rigorous quantum mechanical treatment of the interferometer sequence, considerations of some systematic effects, such as anharmonicity of the confining potential, are more easily incorporated by adopting a semiclassical treatment to compute the wave-packet trajectories and the associated phases. This treatment is valid provided any anharmonicities are sufficiently small so as to not produce significant distortion of the wave packets. A thorough analytic treatment of this range of validity is outside the scope of this work, but explicit numerical simulations have been performed which strongly support the validity of the approximation for the parameter range discussed here. In particular, calculations indicate that significant wave-packet distortion is observed after one trap period of evolution when the anharmonic energy shift is the same order of magnitude as the harmonic potential. For a $\sim$1% anharmonic shift, the overlap between the exactly calculated wave packet and the coherent-state approximation deviates at the level of $\sim 10^{-5}$. Given the $\sim 10^{-4}$ anharmonic contribution considered here, any wave-packet distortion will be entirely negligible. Thus the coherent-state formalism described above can be applied to compute the corresponding visibility (Sec. II B 2) given trajectories that are computed semiclassically.

The wave-packet trajectories are calculated by considering a particle moving classically under the influence of a general potential of the form

$$V(x,y) = c_1\tilde{x}^2 + c_2\tilde{y}^2 + c_3\tilde{x}\tilde{y} + c_4\tilde{x}^4 + c_5\tilde{y}^4 + c_6\tilde{x}^2\tilde{y}^2 + c_7\tilde{x}\tilde{y}^3 + c_8\tilde{x}^3\tilde{y}, \tag{17}$$

where I have defined $\tilde{x} = x/R$, $\tilde{y} = y/R$, with R the characteristic size of the system under consideration (I take this to be the magnitude of the initial real-space displacement from the trap center, d). Other terms of the order of $\leqslant 4$ (e.g., x^3, xy^3, etc.) have been omitted from the present analysis as they are unlikely to arise in common experimental configurations due to symmetry considerations. For example, patch potentials or electrode construction imperfections in linear Paul traps are unlikely to produce such terms—similar arguments apply to optical or magnetic traps for neutral atoms. The effects of these omitted terms were also studied and found to be very similar to that of other anharmonicities, but they are not presented here. The size of the anharmonic terms considered is discussed later.

The acceleration is calculated as $\vec{a}(t) = -\vec{\nabla}V[x(t), y(t)]/m$ and the equations of motion are numerically integrated. In the ideal case, $c_1 = c_2$ are the only nonzero coefficients and the wave-packet trajectories can be expressed analytically. Equations (18)–(24) describe the trajectories while incorporating the following imperfections (cf. Fig. 2): $\theta_{\rm com}$, a common misalignment of the momentum kicks from the nominal axis defining the kick directions, while keeping the kicks opposite to each other; $\theta_{\rm rel}$, a relative misalignment of the momentum kicks with respect to each other; $\theta_{\rm disp}$, a misalignment of the initial displacement; $v_{\rm com}$, a velocity component common to both wave packets; and $\omega_x \neq \omega_y$, a mismatch of the trap

frequencies,

$$x^{\pm}(t) = x_0^{\pm}\sin(\pm\omega_x t + \gamma^{\pm}), \tag{18}$$

$$y^{\pm}(t) = y_0^{\pm}\cos(\xi^{\pm}\omega_y t - \psi^{\pm}), \tag{19}$$

$$\gamma^{\pm} = \sin^{-1}\left[\frac{d\sin(\theta_{\rm disp})}{x_0^{\pm}}\right], \tag{20}$$

$$\psi^{\pm} = \cos^{-1}\left[\frac{d\cos(\theta_{\rm disp})}{y_0^{\pm}}\right], \tag{21}$$

$$x_0^{\pm} = \sqrt{\frac{[v_{x,\rm com} \pm v_{\rm SDK}\cos(\theta_{\rm com}\mp\theta_{\rm rel})]^2}{\omega_x^2} + [d\sin(\theta_{\rm disp})]^2}, \tag{22}$$

$$y_0^{\pm} = \sqrt{\frac{[v_{y,\rm com} \pm v_{\rm SDK}\sin(\theta_{\rm com}\mp\theta_{\rm rel})]^2}{\omega_y^2} + [d\cos(\theta_{\rm disp})]^2}, \tag{23}$$

$$\xi^{\pm} = \mathrm{sgn}[v_y^{\pm}(0)]. \tag{24}$$

The $\pm$ superscripts label wave packets that are initially moving in $\pm x$. $v_{\rm SDK}$ denotes the magnitude of the velocity imparted by the SDKs that split the wave packets, i.e.,

$$v_{\rm SDK} = \sqrt{\frac{2\hbar\omega}{m}}n_{\rm k}\eta. \tag{25}$$

Note that the expression for the initial velocity $v_y^{\pm}(0)$ is not explicitly written, but can be readily calculated given the imperfections that are present.

At each point in the trajectory, a corresponding coherent state can be calculated as [cf. Eqs. (2) and (3)]

$$\alpha_x(t) = \sqrt{\frac{m\omega}{2\hbar}}x(t) + i\sqrt{\frac{1}{2m\omega\hbar}}p_x(t). \tag{26}$$

The direct analogy between the classical trajectory and the associated coherent state facilitates quick calculation of the effects of experimental imperfections.

With the wave-packet trajectories in hand, one can use the path-integral formulation [34,35] to calculate the associated accumulated phase, which is given by integrating the classical action and dividing by Planck's constant:

$$\phi(t) - \phi(0) = \frac{1}{\hbar}\int_0^t \mathcal{L}(t')dt'. \tag{27}$$

Oscillation in a harmonic potential for an integer number of trap periods produces no net phase,

$$\phi(n2\pi/\omega) = \frac{m}{2\hbar}\int_0^{n2\pi/\omega} \dot{x}(t)^2 - \omega^2 x(t)^2 dt = 0. \tag{28}$$

Anharmonicities produce phases which can, in some cases, be found analytically [26] or computed by direct integration of Eq. (27).

B. Interferometer performance

In this section, I discuss the properties that quantify the performance of a TMI. The ways that these properties depend on experimental imperfections comprise the systematic effects studied here.

1. Phase

The phase difference between two wave packets, $\delta\phi$, is the critical quantity of interest in any interferometer; the interferometric study of a particular interaction Hamiltonian is typically achieved by measuring the phase difference that it produces. Any additional phase difference arising from other Hamiltonian terms should be considered as a systematic effect and is the first metric that I use to quantify interferometer performance. In particular, it is less important that the phase difference be exactly zero, but rather that it is insensitive to experimental parameters that are not of interest. One such parameter of obvious importance is time—if the phase difference changes rapidly in time, the interferometer phase will be sensitive to both the precision of the experimental timing and the stability of the oscillation period of the confining potential. As such, I define the following as a metric of interferometer stability:

$$\xi \equiv \frac{\partial\delta\phi(t)}{\partial t}. \tag{29}$$

Here, ξ is evaluated at the point of recombination of the wave packets, where the visibility is highest. This brings us to a second important measure of interferometer performance.

2. Visibility

Interferometer visibility is a measure of the change in signal (for a TMI, the change in $P_\uparrow$) as a function of $\delta\phi$ and the measurement sensitivity is proportional to the visibility. Optimal visibility is achieved when the wave packets are perfectly overlapped in phase space at recombination. An expression for the visibility in the case of a 1D interferometer described above can be derived by evaluating Eq. (10). For clarity, I will insert the wave-packet-dependent interferometer phase, $\pm\phi/2$ [36]. This is in addition to the phases $\phi_{\uparrow,\downarrow}$ arising from the displacements intrinsic to the interferometer sequence,

$$|\psi_f\rangle = \tfrac{1}{2}[e^{i\phi/2}e^{i\phi_\downarrow}|\alpha+\delta_\downarrow\rangle\otimes(|\uparrow\rangle - |\downarrow\rangle) \tag{30}$$

$$+ e^{-i\phi/2}e^{i\phi_\uparrow}|\alpha+\delta_\uparrow\rangle\otimes(|\uparrow\rangle + |\downarrow\rangle)]. \tag{31}$$

The interferometer signal is found by making a projective measurement onto $|\uparrow\rangle$ and averaging over a thermal distribution. Doing so gives the following expression:

$$P_\uparrow(\bar{n}) = \int \frac{e^{-|\alpha|^2/\bar{n}}}{\pi\bar{n}}|\langle\uparrow|\psi_f\rangle|^2 d^2\alpha \tag{32}$$

$$= \frac{1}{2} + \frac{1}{2}e^{-|\frac{\delta}{2}|^2(\bar{n}+2)}\cos(\Phi+\theta), \tag{33}$$

where I have defined $\delta \equiv \delta_\downarrow - \delta_\uparrow$, and θ is an additional phase prescribed by δ. The visibility can be quickly identified as

$$\mathcal{V} = e^{-|\frac{\delta}{2}|^2(\bar{n}+2)}. \tag{34}$$

This treatment can be easily extended to the 2D case, where each axis has an associated $\bar{n}$ and δ which, in general, differ between axes. The two axes can be treated independently and

the associated visibilities multiplied together (which is equivalent to adding δ_x and δ_y in quadrature to give the separation of the wave packets in the 4D phase space associated with the two axes).

Aside from the maximum visibility of the interferometer, it is again interesting to note sensitivity to experimental parameters such as the trap frequency. At recombination, the visibility varies in time with a Gaussian temporal profile. I will use the corresponding standard deviation $\sigma_{\mathcal{V}}$, in units of the trap period, as a measure of sensitivity to the trap frequency.

3. Enclosed area

One final metric that I shall consider is specific to the case of a Sagnac interferometer. Rotation of the interferometer produces a phase on each wave packet,

$$\Phi = \frac{2m}{\hbar}\vec{\mathcal{A}}\cdot\vec{\Omega}, \tag{35}$$

where m is the particle mass, $\vec{\mathcal{A}}$ is the enclosed area, and $\vec{\Omega}$ is the rotation rate. I will assume that $\vec{\mathcal{A}}$ is aligned with $\vec{\Omega}$. The interferometer phase is proportional to the vector difference of the enclosed areas, $\delta\vec{\mathcal{A}}$. I assume that the areas enclosed by the wave packets are opposite, so $\delta\vec{\mathcal{A}}$ is equivalent to the scalar sum of the areas. Thus the enclosed area (often expressed, together with particle energy, as a "scale factor") characterizes the sensitivity of a Sagnac interferometer and any systematic that changes $\delta\vec{\mathcal{A}}$ is important to consider as it could jeopardize precision and accuracy.

The enclosed area for each wave packet is readily calculated from the trajectories according to Green's theorem,

$$\vec{\mathcal{A}} = \frac{1}{2}\int_0^t \vec{r}(t')\times\vec{v}(t')dt' = \frac{1}{2m}\int_0^t \vec{L}(t')dt', \tag{36}$$

where $\vec{L}$ is the wave-packet angular momentum. In general, this is calculated numerically, but for central potentials, we can write the difference in enclosed areas as (cf. Fig. 1)

$$\delta\vec{\mathcal{A}} = \vec{\mathcal{A}}_1 - \vec{\mathcal{A}}_2 = \frac{t}{2m}\delta\vec{L}, \tag{37}$$

where t is the oscillation period and $\delta\vec{L}$ is the difference in angular momentum of the wave packets.

III. SYSTEMATIC EFFECTS

From here on, I will use x_0 and y_0 to refer to the amplitudes of motion. In the absence of imperfections, these equate to $p_x/m\omega_x$ and d, respectively. Throughout this section, I shall consider two specific scenarios:

(A) $^{138+}$Ba ion trapped in an $\omega = 2\pi \times 100$ kHz potential with $x_0 = 1$ μm and $y_0 = 100$ μm. $\bar{n} = 0$ or $\bar{n} = 125$, corresponding to a temperature of 0.6 mK.

(B) ^{87}Rb atom trapped in an $\omega = 2\pi \times 10$ Hz potential with $x_0 = y_0 = 200$ μm. $\bar{n} = 416$, corresponding to a temperature of 200 nK.

A. Individual imperfections

Here I will examine the effect of a single experimental imperfection on the metrics previously listed as quantifying the interferometer performance. A summary of the imperfections considered and the metrics affected is provided in Fig. 2. Also shown are real-space trajectories of the wave packets in the presence of such (greatly exaggerated) imperfections, in order to aid intuition.

1. Ideal case

In the ideal case, it is straightforward to calculate all the performance metrics. The phase difference $\delta\phi$ is zero at all times by symmetry. The visibility $\mathcal{V}$ is 1 at recombination. The value of $\delta\vec{\mathcal{A}}$ is provided by Eq. (37) and the sensitivity to experimental imperfections is clear.

Close to recombination, the wave packets are separated in real space along one axis [37]. It is then straightforward to write the time evolution of the visibility. Using Eq. (26), the wave-packet trajectories and the small-angle approximation give the coherent state at a time t away from recombination,

$$\alpha(t) = \pm\sqrt{\frac{m\omega}{2\hbar}}x_0\omega t, \tag{38}$$

where "±" refers to the two wave packets. The separation in phase space, δ, is given by twice this amount. We can use Eq. (34) to write

$$\mathcal{V} = \exp\left[-m\omega^3 x_0^2 t^2(\bar{n}+2)/2\hbar\right]. \tag{39}$$

The temporal width of the visibility peak is then

$$\sigma_{\mathcal{V}} = \sqrt{\frac{\hbar}{m\omega^3 x_0^2(\bar{n}+2)}}. \tag{40}$$

A change in the oscillation frequency, $d\omega$, will cause inaccurate recombination and a reduction in visibility,

$$d\mathcal{V} = 1 - \exp\left[-\frac{2\pi^2 m\omega x_0^2(\bar{n}+2)}{\hbar}\left(\frac{d\omega}{\omega}\right)^2\right]. \tag{41}$$

As an example, in both scenarios (A) and (B), $d\omega/\omega = 10^{-5}$ produces $d\mathcal{V} \sim 10^{-5}$ ($\sim 10^{-3}$) for $\bar{n} = 0$ ($\bar{n} = 124$). To reduce the visibility to 10%, $d\omega/\omega \sim 10^{-3}$ ($\sim 10^{-4}$) is required for $\bar{n} = 0$ ($\bar{n} = 124$).

Note that the above analysis is for a single orbit; for multiple orbits, $d\omega$ is multiplied by the number of orbits.

2. Misalignments $\theta_{\rm com}$, $\theta_{\rm rel}$, and $\theta_{\rm disp}$

These imperfections are illustrated in Figs. 2(b)–2(d). They incorporate misalignment of the directions of the momentum kicks imparted to split the wave packet and of the initial real-space displacement of the wave packet [38]. With these imperfections, the trajectories are ellipses which are described by Eqs. (18)–(24).

With any of these imperfections, $\delta\phi$, $\mathcal{C}$, and $\sigma_{\mathcal{C}}$ are unaffected, but the enclosed areas are modified to give [cf. (37)]

$$\delta\vec{\mathcal{A}} = \frac{2\pi d p_x}{m\omega}\cos\theta_{\rm com}\cos\theta_{\rm rel}\cos\theta_{\rm disp}. \tag{42}$$

Either $\theta_{\rm com}$ or $\theta_{\rm disp}$ breaks the symmetry of the wave-packet trajectories, which produces a phase difference during the oscillations; however it takes the form $\delta\phi(t) \sim \sin^2(\omega t)$ such that $\xi = 0$ at recombination and $\delta\phi$ is insensitive to changes in the trapping frequency to first order.

3. Common velocity $v_{\rm com}$

This imperfection is illustrated in Fig. 2(e). As with the previous systematic effects, the visibility and accumulated phase are unaffected. The area enclosed by each wave packet is modified according to Eq. (37), but $\delta\vec{\mathcal{A}}$ remains unchanged.

This experimental imperfection is not completely benign, however; a common initial velocity along $\pm\hat{x}$ makes the phase difference at recombination, while equal to zero, sensitive to the trap frequency. Using Eqs. (27) and (18)–(24), the phase difference is given by

$$\delta\phi(t) = \frac{2v_{x,\rm com}p_{\rm SDK}}{\hbar\omega}\sin(\omega t)\cos(\omega t), \tag{43}$$

where $p_{\rm SDK} = mv_{\rm SDK}$. The time derivative at $t = 2\pi/\omega$ (equivalently, at $t = 0$) can be computed directly from this formula and is nonzero. Alternatively, one can note that

$$\xi \equiv \left.\frac{\partial\delta\phi(t)}{\partial t}\right|_{t=0} = \frac{1}{\hbar}[\mathcal{L}_1(0) - \mathcal{L}_2(0)] \tag{44}$$

$$= \frac{1}{\hbar}[T_1(0) - T_2(0)] \tag{45}$$

$$= \frac{2v_{x,\rm com}p_{\rm SDK}}{\hbar}. \tag{46}$$

For a change in trap frequency of $d\omega$, the change in the phase difference is

$$d\delta\phi(t = 2\pi/\omega) = \frac{4\pi v_{x,\rm com}p_{\rm SDK}}{\hbar\omega}\frac{d\omega}{\omega}. \tag{47}$$

It should be noted that this error is smaller for higher trap frequencies and increases with $p_{\rm SDK}$ (which is desired for greater interferometric sensitivity). Assuming $v_{x,\rm com}$ equal to $v_{\rm rms}$ for scenarios (A) and (B), and $d\omega/\omega = 10^{-5}$, produces a phase difference of $\delta\phi \sim \pi/10$. Again, this treatment assumes a single orbit; the accumulated phase difference is multiplied by the number of orbits.

In practice, $v_{x,\rm com}$, and hence ξ, will likely have a range of values that is symmetrically distributed around zero. In this case, the presence of $d\omega$ will not affect the mean value of $\delta\phi$, but will, upon taking an ensemble average, reduce the visibility and hence the precision with which $\delta\phi$ can be measured.

4. Trap frequency mismatch $\omega_x \neq \omega_y$

This imperfection is illustrated in Fig. 2(f). Note that I am assuming that the principal axes of the trap are aligned with the Cartesian axes. Rotation of these axes relative to each other changes the effects of some imperfections. In particular, a trap frequency mismatch takes on the character of other imperfections, most intuitively a coupling between the axes (Sec. III A 6).

Again, by symmetry, neither $\delta\phi$ nor $\mathcal{C}$ are affected by a trap frequency mismatch. However, $\delta\vec{\mathcal{A}}$ is affected as the confining potential is no longer central. Let ω_y change by an amount $d\omega$. Using Eq. (36), the enclosed area is, to first order in $d\omega$,

$$\mathcal{A} = \frac{x_0y_0(2\omega_x + d\omega)}{4d\omega}\sin(2\pi d\omega/\omega_x) \tag{48}$$

$$\approx \pi x_0y_0(1 + d\omega/\omega_x). \tag{49}$$

It should also be noted that the trajectories are no longer closed. In particular, for a single orbit, a displacement of

$$\frac{dy}{y_0} = 1 - \cos(2\pi\omega_y/\omega_x) \approx 2\pi^2\left(\frac{d\omega}{\omega}\right)^2 \tag{50}$$

relative to the initial position is produced. Such a shift is unlikely to be problematic; e.g., in scenario (A), a 10^{-5} mismatch between frequencies produces a negligible 0.1 pm of displacement per orbit. Of course, significantly larger trap instabilities should be avoided.

5. Anharmonicity $V \sim x^4, y^4, x^2y^2$

This imperfection is illustrated in Fig. 2(g) and consists of modifying the trapping potential [Eq. (17)] to contain terms proportional to x^4, y^4, and x^2y^2. I ignore terms such as $V \sim xy^3, x^3y$ as these are generally negligible due to the symmetry of the apparatus used to generate the trapping potential. The only metric impacted is the enclosed area. The resulting trajectories are most similar to the case with $\omega_x \neq \omega_y$ (Sec. III A 4) and suffer from the same problem that the recombination is offset from the initial position.

6. Axis coupling $V \sim xy$

This imperfection is illustrated in Fig. 2(h). It is a modification of the trapping potential to include coupling between the two spatial axes. This is by far the most detrimental imperfection considered here and the only one that causes the orbits not to close. As such, multiple metrics of the interferometer are affected. Unlike the other systematics considered, the symmetry of the trajectories is broken in both x and y, meaning that the recombination is affected.

B. Multiple imperfections

I will now assess how detrimental multiple imperfections might be in an actual experiment, with explicit quantitative analysis in the context of scenarios (A) and (B).

Combinations of multiple imperfections have the potential to cause significant deterioration in performance. As an example, in the previous section it was shown that a potential term of the form $V \sim xy$ could reduce the visibility. Such a potential is in fact identical to one with mismatched trap frequencies, rotated by $\pi/4$. Indeed, the trajectories produced by $V \sim xy$ can be mimicked by setting $\theta_{\rm disp} = -\theta_{\rm com} = \pi/4$ and $\omega_x \neq \omega_y$. In fact, a combination of $\omega_x \neq \omega_y$ and $\theta_{\rm com}$ can produce a significant reduction in performance.

Similar effects are also seen in the presence of anharmonicity ($V \sim x^4, y^4$). This was shown in previous work for a 1D interferometer [26] where an anharmonic potential together with $v_{x,\rm com}$ affected the interferometer phase. This persists to the 2D case. The presence of $v_{x,\rm com}$ breaks the symmetry of the wave-packet trajectories, which, if the potential is not harmonic, causes the two wave packets to accumulate different phases. A similar effect is observed for an anharmonic potential together with $\theta_{\rm com}$.

It is clear from the foregoing discussion that precise control of the trapping potential is perhaps the most critical factor in ensuring optimal performance of TMIs. To this end, ion traps are particularly well suited—the characteristic length scale of

TABLE I. From left: Imperfection; Representative "typical" value; Change in phase difference with change in this parameter, normalized to the typical value; Value of parameter for which the interferometer visibility drops to 10% with all other parameters kept constant; Value of parameter for which the area difference changes by 10% with all other parameters kept constant. Blank space indicates that no such value was found. See main text for further details.

			10% visibility		
Imperfection, X	Value	$X\frac{\partial\delta\phi}{\partial X}$ (rad)	$\bar{n}=0$	$\bar{n}=124$	10% $\delta\vec{\mathcal{A}}$ change
$\theta_{\rm com}$	20 mrad	0.05			420 mrad
$\theta_{\rm rel}$	20 mrad	0.01			440 mrad
$\theta_{\rm disp}$	20 mrad	6×10^{-4}			420 mrad
$v_{\rm com}$	0.5 m/s	1.8			
ω_y/ω_x-1	10^{-5}	3×10^{-4}		0.04	0.16
$c_4/c_1=c_5/c_1=c_6/c_1$	10^{-4}	0.004		0.05	0.21
c_3/c_1	10^{-4}	0.3	0.013	3×10^{-3}	0.27

ion trap electrodes can easily be many orders of magnitude larger than the oscillation size, which helps guarantee that anharmonicities ($V\sim x^4, y^4$) are extremely small. Finite element simulation of potentials generated by macroscopic (∼1–10 mm) traps indicates that values of $c_{4,5,6}$ that are a factor of $\sim10^4$ smaller than $c_{1,2}$ can easily be achieved over a 100 μm region. Theoretical treatment of trap anharmonicity suggests that for macroscopic traps this is a conservative estimate [39]. Symmetry dictates that $c_3/c_{1,2}$ should be zero, but a value of 10^{-4} is assumed for the present analysis. As previously mentioned, stabilization [40] and matching of the trap frequencies will also dramatically reduce any potential systematic effects. Additionally, ensuring that the axes defining the real- and momentum-space displacements are aligned with the principal axes of the trap helps mitigate deleterious effects due to trap frequency mismatch. Regardless of the experimental realization, it is clear that accurate interferometry will depend on precise characterization of the trapping potential and will be the subject of future investigation.

I now quantitatively examine interferometer performance in a situation where all imperfections are present. I consider scenario (A). In addition to the previously stated parameters, the assumed imperfections are shown in Table I, and the resulting interferometer metrics for $\bar{n}=0\,(\bar{n}=124)$ are as follows:

(a) $\mathcal{V}=1.000\,(0.997)$
(b) $\delta\vec{\mathcal{A}}/\delta\vec{\mathcal{A}}_{\rm ideal}=0.999\,(0.999)$
(c) $\xi=1.3\,{\rm rad/ns}\,(1.3\,{\rm rad/ns})$
(d) $\sigma_{\mathcal{V}}=2\times10^{-3}\,(4\times10^{-4})$.

The quoted values are very promising. Excellent visibility is achieved and there is negligible change in the enclosed area. The value of ξ characterizes the sensitivity to changes in the trap frequency, indicating that a 10^{-5} fractional change would result in a 9 mrad change in the phase difference. For comparison, with the same parameters a measurement of the Earth's rotation rate would produce a phase difference of around 80 mrad. The deterioration of the visibility from such a change in trap frequency, encoded in $\sigma_{\mathcal{C}}$, is seen to be much less significant. It should also be noted that absolute accuracy in, e.g., $\delta\vec{\mathcal{A}}$ may not be required as the interferometer sensitivity can, in some cases, be calibrated to compensate for such an effect. Drifts in such parameters, however, are intrinsically more problematic.

Performing a similar analysis for scenario (B) is also promising—the metrics are very comparable, with one notable difference: the estimated visibility is around 75% due to the higher value of $\bar{n}$; however, this does not present a significant deterioration in performance and could be mitigated by operating at a lower temperature. The disparity in trap frequency also means that the value for ξ is comparable only when scaled according to the trap period; scenario (B) has comparable requirements on the fractional stability of ω, but, of course, less stringent timing requirements.

While it seems that interferometer performance is not jeopardized by the stated imperfections, it is also useful to consider more generally how resilient the interferometer performance is. Some aspects of this analysis are shown in Table I.

Perhaps the most obvious consideration is how the interferometer phase depends on the stated imperfections. The third column of Table I shows the gradient of $\delta\phi$ with respect to the stated imperfection, normalized to the size of that imperfection. This means, for example, that doubling $\theta_{\rm com}$ from 20 to 40 mrad changes $\delta\phi$ by 0.05 rad. $\theta_{\rm com}$, $v_{\rm com}$, and c_{xy}/c_{x2} show notable effects on the phase difference. $v_{\rm com}$ is unlikely to have a nonzero mean value so averaging will likely remove any effect, at the expense of visibility. Reducing noise in $\delta\phi$ associated with $\theta_{\rm com}$ and c_{xy}/c_{x2} to around 1 mrad would require stabilization of these parameters to around 0.4 mrad and 3×10^{-7}, respectively.

The fourth column of Table I lists the size of the imperfection that reduces the visibility of the interferometer to 10%. Again, it is seen that the fidelity of the trapping potential is the most important aspect to control, particularly for the case of thermal states where sensitivity of the visibility is much higher.

The last column of Table I lists the size of imperfection that changes $\delta\vec{\mathcal{A}}$ by 10%. This parameter is again very robust, being largely unaffected by any of the parameters considered.

It should of course be noted that the presented parameter space is large and the parameters are interrelated so the dependence on such imperfections can be significantly more complex than the examples given here for illustration. Additionally, reductions of visibility due to the distribution of values of $v_{\rm com}$ given by the finite wave-packet temperature are not shown here, but may be important to consider when examining a specific interferometer.

IV. CONCLUSIONS

In this paper, I have analyzed a number of experimental imperfections which could mitigate the performance of a trapped matter-wave interferometer. In particular, 2D interferometry increases the number of possible experimental imperfections and introduces ways that these may couple to each other. It is seen that systematic effects arise in particular when the symmetry between the two wave packets is broken, for example, by the presence of a contribution to the trapping potential of the form $\sim xy$, or by a mismatch in trapping frequencies together with a misalignment of the beam-splitter operation. However, my analysis indicates that with good control of the trapping potential, it is possible to realize precise and robust interferometer operation. This conclusion applies to apparatuses based on either ultracold atoms or ions, despite considerable disparity between the associated experimental parameters.

ACKNOWLEDGMENTS

I would like to thank Paul Hamilton and Wes Campbell for useful discussions and careful reading of the manuscript. This work was supported by the Office of Naval Research (Award No. N000141712256) and the Defense Advanced Research Projects Agency (Award No. D18AP00067).

[1] A. D. Cronin, J. Schmiedmayer, and D. E. Pritchard, Rev. Mod. Phys. **81**, 1051 (2009).
[2] S. Fray, C. A. Diez, T. W. Hänsch, and M. Weitz, Phys. Rev. Lett. **93**, 240404 (2004).
[3] G. Rosi, G. D'Amico, L. Cacciapuoti, F. Sorrentino, M. Prevedelli, M. Zych, C. Brukner, and G. M. Tino, Nat. Commun. **8**, 15529 (2017).
[4] C. Overstreet, P. Asenbaum, T. Kovachy, R. Notermans, J. M. Hogan, and M. A. Kasevich, Phys. Rev. Lett. **120**, 183604 (2018).
[5] G. Rosi, F. Sorrentino, L. Cacciapuoti, M. Prevedelli, and G. M. Tino, Nature (London) **510**, 518 (2014).
[6] F. Riehle, T. Kisters, A. Witte, J. Helmcke, and C. J. Bordé, Phys. Rev. Lett. **67**, 177 (1991).
[7] T. L. Gustavson, A. Landragin, and M. A. Kasevich, Classic. Quantum Grav. **17**, 2385 (2000).
[8] B. Barrett, R. Geiger, I. Dutta, M. Meunier, B. Canuel, A. Gauguet, P. Bouyer, and A. Landragin, C. R. Phys. **15**, 875 (2014).
[9] I. Dutta, D. Savoie, B. Fang, B. Venon, C. L. Garrido Alzar, R. Geiger, and A. Landragin, Phys. Rev. Lett. **116**, 183003 (2016).
[10] W. F. Holmgren, M. C. Revelle, V. P. A. Lonij, and A. D. Cronin, Phys. Rev. A **81**, 053607 (2010).
[11] R. H. Leonard, A. J. Fallon, C. A. Sackett, and M. S. Safronova, Phys. Rev. A **92**, 052501 (2015).
[12] R. Trubko, M. D. Gregoire, W. F. Holmgren, and A. D. Cronin, Phys. Rev. A **95**, 052507 (2017).
[13] M. Jaffe, P. Haslinger, V. Xu, P. Hamilton, A. Upadhye, B. Elder, J. Khoury, and H. Müller, Nat. Phys. **13**, 938 (2017).
[14] R. H. Parker, C. Yu, W. Zhong, B. Estey, and H. Müller, Science **360**, 191 (2018).
[15] N. F. Ramsey, Phys. Rev. **78**, 695 (1950).
[16] M. Jacquey, A. Miffre, M. Büchner, G. Trénec, and J. Vigué, Europhys. Lett. **75**, 688 (2006).
[17] F. Sorrentino, Q. Bodart, L. Cacciapuoti, Y.-H. Lien, M. Prevedelli, G. Rosi, L. Salvi, and G. M. Tino, Phys. Rev. A **89**, 023607 (2014).
[18] A. S. Arnold, C. S. Garvie, and E. Riis, Phys. Rev. A **73**, 041606(R) (2006).
[19] B. E. Sherlock, M. Gildemeister, E. Owen, E. Nugent, and C. J. Foot, Phys. Rev. A **83**, 043408 (2011).
[20] P. Navez, S. Pandey, H. Mas, K. Poulios, T. Fernholz, and W. von Klitzing, New J. Phys. **18**, 075014 (2016).
[21] Y. Zhou, I. Lesanovsky, T. Fernholz, and W. Li, arXiv:1811.11107.
[22] J. H. T. Burke and C. A. Sackett, Phys. Rev. A **80**, 061603(R) (2009).
[23] R. Cheng, T. He, W. Li, and A. Smerzi, J. Mod. Phys. **07**, 2043 (2016).
[24] W. C. Campbell and P. Hamilton, J. Phys. B **50**, 064002 (2017).
[25] C. A. Sackett, E. Moan, and Z. Luo, in *Optical, Opto-Atomic, and Entanglement-Enhanced Precision Metrology*, edited by S. M. Shahriar and J. Scheuer (SPIE, Bellingham, WA, 2019).
[26] R. H. Leonard and C. A. Sackett, Phys. Rev. A **86**, 043613 (2012).
[27] G. Sagnac, C. R. Acad. Sci. **157**, 708 (1913).
[28] R. Stevenson, M. R. Hush, T. Bishop, I. Lesanovsky, and T. Fernholz, Phys. Rev. Lett. **115**, 163001 (2015).
[29] Y. Che, F. Yao, H. Liang, G. Li, and X. Wang, Phys. Rev. A **98**, 053609 (2018).
[30] E. R. Moan, R. A. Horne, T. Arpornthip, Z. Luo, A. J. Fallon, S. J. Berl, and C. A. Sackett, arXiv:1907.05466.
[31] D. S. Durfee, Y. K. Shaham, and M. A. Kasevich, Phys. Rev. Lett. **97**, 240801 (2006).
[32] D. Savoie, M. Altorio, B. Fang, L. A. Sidorenkov, R. Geiger, and A. Landragin, Sci. Adv. **4**, eaau7948 (2018).
[33] G. Tackmann, P. Berg, C. Schubert, S. Abend, M. Gilowski, W. Ertmer, and E. M. Rasel, New J. Phys. **14**, 015002 (2012).
[34] J. J. Sakurai and J. Napolitano, *Modern Quantum Mechanics*, 2nd ed. (Cambridge University Press, Cambridge, 2017).
[35] Pippa Storey and Claude Cohen-Tannoudji, J. Phys. II (France) **4**, 1999 (1994).
[36] The origin of this phase is unspecified and depends on the exact details of the interferometer. It may derive from a Hamiltonian term involving the internal states, which I do not consider here.
[37] Recall that a second SDK removes the initial momentum so that the wave packets are not significantly separated along either axis in velocity space.
[38] I note that in many experimental schemes, θ_{rel} is unlikely to occur, but I include it for the sake of generality.
[39] X. Luo, X. Zhu, K. Gao, J. Li, M. Yan, L. Shi, and J. Xu, Appl. Phys. B **62**, 421 (1996).
[40] K. G. Johnson, J. D. Wong-Campos, A. Restelli, K. A. Landsman, B. Neyenhuis, J. Mizrahi, and C. Monroe, Rev. Sci. Instrum. **87**, 053110 (2016).